



University of Kentucky
UKnowledge

Theses and Dissertations--Chemistry

Chemistry

2017

Energetic Effects of Hole Transporting Materials on the Performance of Organometal Halide Perovskite Photovoltaic Cells

So Min Park

University of Kentucky, thals0819@gmail.com

Digital Object Identifier: <https://doi.org/10.13023/ETD.2017.022>

[Right click to open a feedback form in a new tab to let us know how this document benefits you.](#)

Recommended Citation

Park, So Min, "Energetic Effects of Hole Transporting Materials on the Performance of Organometal Halide Perovskite Photovoltaic Cells" (2017). *Theses and Dissertations--Chemistry*. 71.

https://uknowledge.uky.edu/chemistry_etds/71

This Master's Thesis is brought to you for free and open access by the Chemistry at UKnowledge. It has been accepted for inclusion in Theses and Dissertations--Chemistry by an authorized administrator of UKnowledge. For more information, please contact UKnowledge@lsv.uky.edu.

STUDENT AGREEMENT:

I represent that my thesis or dissertation and abstract are my original work. Proper attribution has been given to all outside sources. I understand that I am solely responsible for obtaining any needed copyright permissions. I have obtained needed written permission statement(s) from the owner(s) of each third-party copyrighted matter to be included in my work, allowing electronic distribution (if such use is not permitted by the fair use doctrine) which will be submitted to UKnowledge as Additional File.

I hereby grant to The University of Kentucky and its agents the irrevocable, non-exclusive, and royalty-free license to archive and make accessible my work in whole or in part in all forms of media, now or hereafter known. I agree that the document mentioned above may be made available immediately for worldwide access unless an embargo applies.

I retain all other ownership rights to the copyright of my work. I also retain the right to use in future works (such as articles or books) all or part of my work. I understand that I am free to register the copyright to my work.

REVIEW, APPROVAL AND ACCEPTANCE

The document mentioned above has been reviewed and accepted by the student's advisor, on behalf of the advisory committee, and by the Director of Graduate Studies (DGS), on behalf of the program; we verify that this is the final, approved version of the student's thesis including all changes required by the advisory committee. The undersigned agree to abide by the statements above.

So Min Park, Student

Dr. Kenneth Graham, Major Professor

Dr. Mark Lovell, Director of Graduate Studies

ENERGETIC EFFECTS OF HOLE TRANSPORTING MATERIALS ON THE
PERFORMANCE OF ORGANOMETAL HALIDE PEROVSKITE PHOTOVOLTAIC
CELLS

THESIS

A thesis submitted in partial fulfillment of the requirements
for the degree of Master of Science in the College of Chemistry
at the University of Kentucky

By

So Min Park

Lexington, Kentucky

Director : Dr. Kenneth Graham, Assistant Professor of Chemistry

Lexington, Kentucky

2016

Copyright© So Min Park 2016

ABSTRACT OF THESIS

ENERGETIC EFFECTS OF HOLE TRANSPORTING MATERIALS ON THE PERFORMANCE OF ORGANOMETAL HALIDE PEROVSKITE PHOTOVOLTAIC CELLS

Efficient, inexpensive, lightweight and flexible solar cells are desired to help meet the world's growing energy needs. Organometal halide perovskite (OMHP) photovoltaic (PV) cells have shown dramatic increases in solar cell efficiencies increase over the last 5 years. OMHP PV cells have attracted significant attention due to their broad absorption spectra, high electron and hole mobility, and low production cost. The interface between hole transporting layer (HTL) and perovskite thin films have a significant influence on charge transfer and overall solar cell performance. 2,2',7,7'-tetrakis(N,N-di-p-methoxyphenylamine)9,9'-spirobifluorene (Spiro-OMeTAD) is a small molecule largely used as HTL in perovskite solar cells. However, this material suffers from low charge-carrier mobilities and inappropriate energy level alignments with some perovskites. In this work we investigate the effect of the HTL energetics on the performance of perovskite solar cells. This is accomplished through employing a range of HTLs with varying ionization energies (IEs). We find that the solar cell device performance is relatively insensitive to the IE of the HTL within a 0.4 eV range. We also demonstrate that modification of the HTL surface with different alcohols helps in increasing the solar cell performances.

KEYWORDS: Organometal halide perovskite photovoltaic cells, hole transporting material, charge transfer process

So Min Park

December 14, 2016

ENERGETIC EFFECTS OF HOLE TRANSPORTING MATERIALS ON THE
PERFORMANCE OF ORGANOMETAL HALIDE PEROVSKITE PHOTOVOLTAIC
CELLS

By

So Min Park

Dr. Kenneth Graham

Director of Thesis

Dr. Mark Lovell

Director of Graduate Studies

December 14, 2016

ACKNOWLEDGMENTS

I would like to express my appreciation to my advisor, Dr. Kenneth Graham, for his support and encouragement to make this work possible. I have been always encouraged and energized by his dedication to work and attitude to students with true heart. It was great opportunity for me to have a chance to build a lab which I have not had it before. I would also like to thank Dr. Dong-Sheng Yang, my committee members, Dr. John Anthony and Dr. Yang-Tse Cheng for their help and support. Especially, without DTADIS derivatives hole transporting materials from Dr. John Anthony's lab this work could not be done this far.

Living in different country far away from home was challenge for me at first. Teaching and learning in different language took time for me to adjust and different background major made even harder in my studies. However, discuss problems and study together with friends helped me a lot to understand and it was really valuable time for me. I want to thank all chemistry people and especially, Bidhya Maharjan, Surya Banks, Dr. April French, research group members, and University of Kentucky chemistry department for supporting and advising.

In addition, I want to thank my friend Lauren Hannemann who was my roommate. You always be with me all the moments in my America life even happy or sad times. You and your family's warm heart really touched me and I learned and enjoyed a lot with you.

I thank my family for their love and support always in my life. Thank you my parents who dedicated their life for teaching me to go correct direction and want to say I love you so much father, mother and my younger brother.

LIST OF TABLES

Table 1. PV parameters of adduct solution procedure OMHP PV cells	14
Table 2. PV parameters of conventional PVcells with different ETL	15
Table 3. PV parameters of OMHP PV cells with different MAI, annealing temperature process	17
Table 4. PV parameters of OMHP PV cells with different annealing temperature, drip solution process	18
Table 5. PV parameters of OMHP PV cells with different HTMs	26

LIST OF FIGURES

Figure 1. NREL plot of record PV cell efficiencies for different materials: organometal halide perovskite (OMHP) PV cell efficiencies are highlighted with circle.	2
Figure 2. JV curve showing PV parameters of PV cell.	3
Figure 3. Perovskite crystal structure.	3
Figure 4. OMHP PV cell structure showing the a) inverted and b) conventional.	5
Figure 5. Perovskite processing methods including one step coating (top), two step coating (middle), and solvent engineering (bottom).	7
Figure 6. J-V curves of adduct solution procedure.	14
Figure 7. J-V curves of Lumtec MAI and house MAI.	16
Figure 8. J-V curves of optimized OMHP PV cell.	18
Figure 9. Chemical structure of hole transporting materials (HTMs).	20
Figure 10. UPS energetic spectra for HTMs showing the a) secondary electron cutoff and b) HOMO onset region.	21
Figure 11. Schematic band alignment in OMHP PV cells.	22
Figure 12. UV-vis absorption spectra of different HTLs.	23
Figure 13. J-V characteristic of OMHP PV cells with different HTMs showing the dark (dash and dot), forward (solid), reverse (dash) curves.	25
Figure 14. External quantum efficiency (EQE) spectra of OMHP PV cells.	27
Figure 15. Scanning electron microscope (SEM) images of OMHP PV cells with 5 μm scale bar and inset images 1 μm scale bar.	28

TABLE OF CONTENTS

ACKNOWLEDGMENTS	iii
LIST OF TABLES	iv
LIST OF FIGURES	v
CHAPTER 1 : INTRODUCTION	1
1.1 Opportunities and challenges of PV cells	1
1.2 PV cell operation	2
1.3 Perovskite thin film coating methods	5
1.4 Hole transporting material (HTM) effects on OMHP PV	7
1.5 Research objectives	8
CHAPTER 2 : EXPERIMENTAL METHODS	9
2.1 Materials	9
2.2 Perovskite precursor preparation	9
2.3 Inverted OMHP PV cell device preparation	9
2.4 Instrumental background	11
CHAPTER 3 : OMHP PV CELL DEVICE OPTIMIZATION	13
3.1 Adduct solution procedure	13
3.2 Conventional architecture	14
3.3 Comparison of methylammonium iodide (MAI)	16
CHAPTER 4 : HTM EFFECTS ON OMHP PV PERFORMANCE	19
4.1 Selection of HTMs	19
4.2 Energy levels of HTMs	19
4.3 UV-vis absorption and of HTMs	22
4.4 Device performances of OMHP PV cells	23
4.5 Morphological characterization	27
CONCLUSIONS	28
REFERENCES	29

CHAPTER 1 : INTRODUCTION

1.1 Opportunities and challenges of PV cells

Many of the natural resources we use for energy are limited, but consumption of energy is increasing in the world. To find alternative energy sources, renewable energy has been broadly studied due to its lower pollution and a number of different sources; including geothermal, hydro, ocean, wind, and solar. The cost of photovoltaic (PV) modules have decreased drastically over the past decade, which has resulted in a large increase in the number of PV installation.¹ Total installed PV capacity has increased 180 times more in 2015 than 2004. By the end of 2015, cumulative installed PV capacity reached 200 gigawatts (GW). Research on PV cells started in the 1950s and research efforts have been increasing ever since.² Figure 1. shows plot of record PV efficiencies from national renewable energy laboratory (NREL).³

Photovoltaic cell technology can be divided into three generations. First generation PV cells are made from inorganic silicon. These types of PV cells show good efficiency and high stability. However, high temperatures in silicon purification made the materials expensive and encouraged researchers to seek lower-cost materials. Second generation PV cells include bulk or crystalline thin film silicon, cadmium telluride (CdTe), cadmium sulfide (CdS) and copper indium gallium selenide (CIGS).^{4,5} Some second generation cells have decreased processing or materials cost, but these PV cells typically show lower efficiencies and they are still expensive. Third generation PV cell technologies include solution processable materials such as organic small molecules, polymers, dye sensitized materials, quantum dots, and perovskite materials. These third generation cells primarily include organic PV cell (OPV), dye sensitized PV cell, quantum dot (QD) PV cell, and OMHP PV cells.⁶⁻¹²

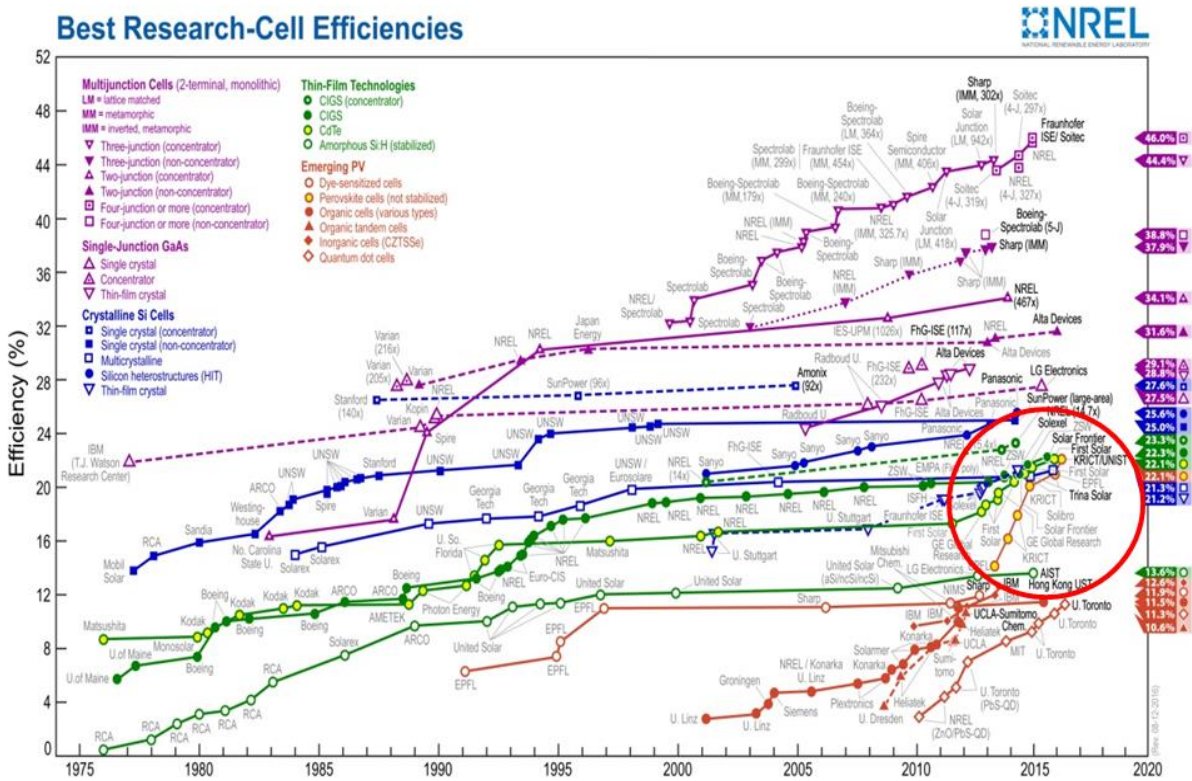


Figure 1. NREL plot of record PV cell efficiencies for different materials: organometal halide perovskite (OMHP) PV cell efficiencies are highlighted with circle.

1.2 PV cell operation

A photovoltaic cell is a device that converts photons into electricity through the photovoltaic effect. At first, light is absorbed by the solar cell and produces electron-hole pairs. These electron-hole pairs separate and the charges are collected by the electrodes. The power conversion efficiency (PCE) is equal to the maximum power output of the solar cell divided by the radiant power incident on the solar cell. The parameters that determine the PCE are the open circuit voltage (V_{oc}), short circuit current density (J_{sc}), and fill factor (FF). The V_{oc} is defined as the maximum voltage that can be generated across the cell upon illumination, which occurs when the device is at an open circuit condition. J_{sc} is defined as the current density at zero voltage. FF is the ratio of the maximum power generated by the

cell to the product of the V_{oc} and J_{sc} as shown in Figure 2. Therefore, increasing the solar cell performance may be accomplished by increase J_{sc} , V_{oc} , and the FF.

$$PCE (\%) = \frac{FF \times J_{sc} \times V_{oc}}{P_{in}} \times 100 \quad (1.1)$$

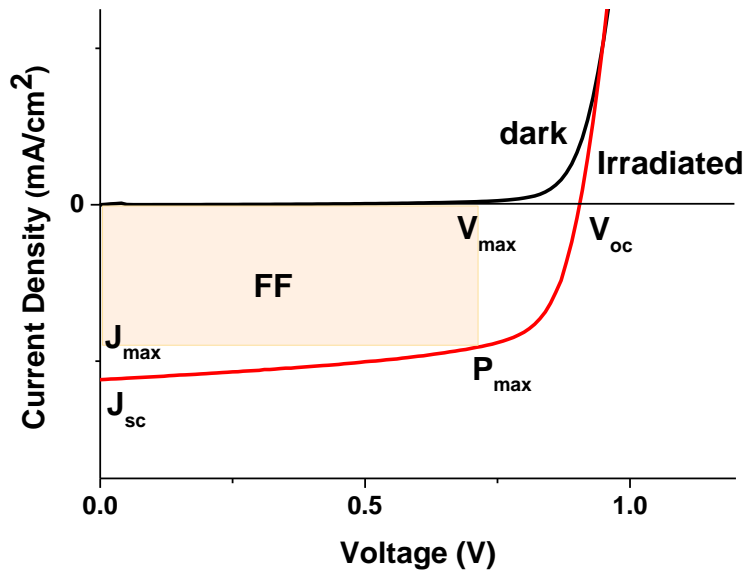


Figure 2. JV curve showing PV parameters of PV cell.

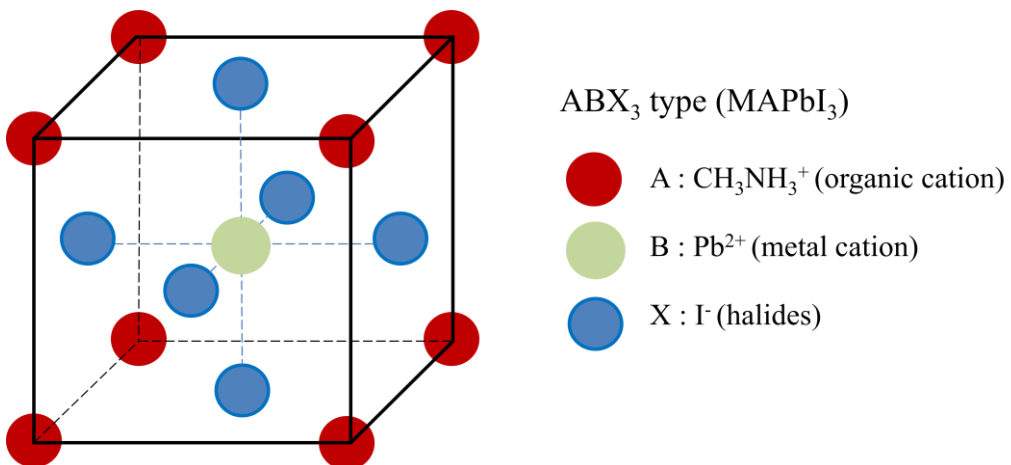


Figure 3. Perovskite crystal structure.

A perovskite has the same generic crystal structure as calcium titanium oxide as shown in Figure 3.¹³ Perovskite materials have been widely studied for optical properties,¹⁴ thermoelectric properties,¹⁵ and electrical conductivity.¹⁶ Most recent research efforts on PVs have focused primarily on OMHPs, and specifically methylammonium lead iodide. These OMHPs have attracted significant research efforts due to their high efficiency and low production cost.¹⁷⁻²⁰ Within the last 7 years, perovskite solar cells have shown dramatic increases in PCE from 3.8% in 2009,²¹ to 22% in 2016 for single-junction cells.²²⁻²⁶

Perovskite solar cells do not require much material, as a two to three hundred nanometer thickness of perovskite layer is sufficient to absorb 80% of incident light as a photo active layer.²⁷ Methylammonium lead iodide (MAPbI₃) absorbs light broadly throughout the visible region, methylammonium lead bromide (MAPbBr₃) and methylammonium chloride (MAPbCl₃) do not. OMHP photovoltaic cell also has ambipolar transport properties with high electron and hole mobility.²⁸ OMHP photovoltaic cell architecture can be either conventional or inverted structure as shown in Figure 4. In conventional cells, a transparent conductive electrode (TCE) is utilized as the bottom layer, where the TCE is usually indium tin oxide (ITO) or fluorine tin oxide (FTO). On top of TCE layer, an electron transporting layer (ETL) is deposited. Commonly used ETL materials include titanium dioxide (TiO₂), C60, or zinc oxide (ZnO).²⁹⁻³² Although TiO₂ is inexpensive, it requires a high sintering temperature of 500 °C, which eliminates the possibility for processing on plastic substrates and increases the energy cost of making the cells. Furthermore, TiO₂ ETL layers tend to show large hysteresis in the J-V characteristics.

In inverted perovskite solar cells, the hole transporting layer (HTL) is deposited between the TCE and the perovskite active layer. The most common material for the HTL is the conducting polymer blend poly(3,4-ethylenedioxythiophene):polystyrene sulfonate

(PEDOT:PSS), in part due to its good hole transporting ability and stability in devices.^{33,34} Usually other HTL materials are π -conjugated organic molecules and they are processed from common organic solvents such as chloroform (CF), chlorobenzene (CB) or dichlorobenzene (DCB). The perovskite film is usually spun cast from dimethylformamide (DMF) or dimethyl sulfoxide (DMSO). Fortunately, the π -conjugated organic HTL materials are generally not soluble in these solvents.

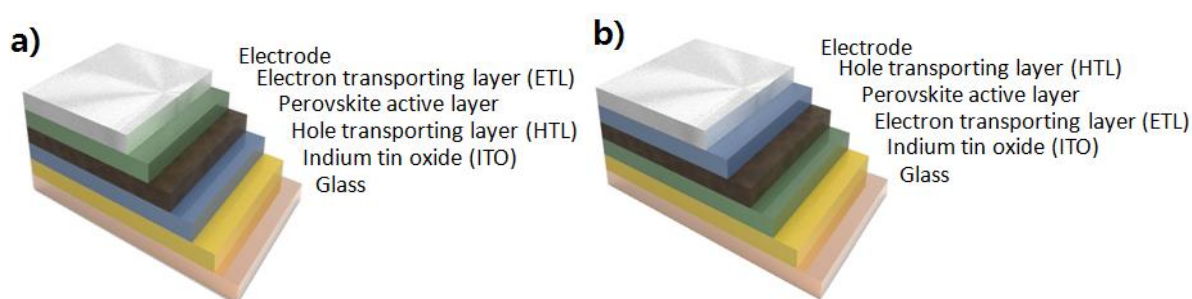


Figure 4. OMHP PV cell structure showing the a) inverted and b) conventional.

To improve charge extraction and minimize charge recombination, charge transfer processes between interlayers are very important. Typically, the perovskite thin film is sandwiched between a HTL and ETL. Each transport layer needs to have good charge carrier mobility, sufficient conductivity as well as well-aligned energy level with other layers to help charge transfer to occur efficiently and without energy losses.^{35,36}

1.3 Perovskite thin film coating methods

One of the major variables that influences the performance of perovskite photovoltaic cell is the morphology of the perovskite layer. If the perovskite layer is not homogeneously coated on the substrate, light can pass through the layer without any absorption and this can decrease device photo current. More importantly, without a continuous perovskite film shunts

or shorts can form between the electrodes. To improve OMHPs film morphologies, many different types of perovskite thin film processing methods have been developed.³⁷⁻⁴⁰ These include one-step coating, two-step coating, and a “solvent engineering” process, as depicted schematically in Figure. 5.

One of the processing methods is perovskite single step solution coating.⁴¹⁻⁴⁵ In this process, metal halide (e.g. PbI_2) and organic halide (e.g. $\text{CH}_3\text{NH}_3\text{I}$) are dissolved in an organic solvent. After spin coating, the device is placed directly on a hot plate with 100 °C annealing temperature to induce crystallization of the perovskite.

Other method is a two step coating process. In contrast with the one step method, two step coating process has been developed recently and showed several enhancements in the morphology of perovskite layer.⁴⁶⁻⁴⁸ In the sequential deposition method, Burschka et al. introduced lead iodide (PbI_2) to nanoporous TiO_2 film and transformed them into the perovskite by exposing it to a solution of methylammonium iodide (MAI).⁴⁹ Perovskite morphology was greatly increased because of direct contact between nanoporous TiO_2 and MAI. This method showed both increased efficiency and reproducibility.

Additionally, many groups have tried solvent engineering techniques to improve morphologies of films. Seok and his co-workers introduced solvent drip during spin coating of perovskite precursor to get extremely uniform and dense layer.⁵⁰ Li et al. demonstrated controlled morphology of film by mixing DMF and DMSO solutions. DMSO coordinates strongly with PbI_2 , and this makes the perovskite crystal grow slower, which results in homogeneous of perovskite thin films morphology.⁵¹

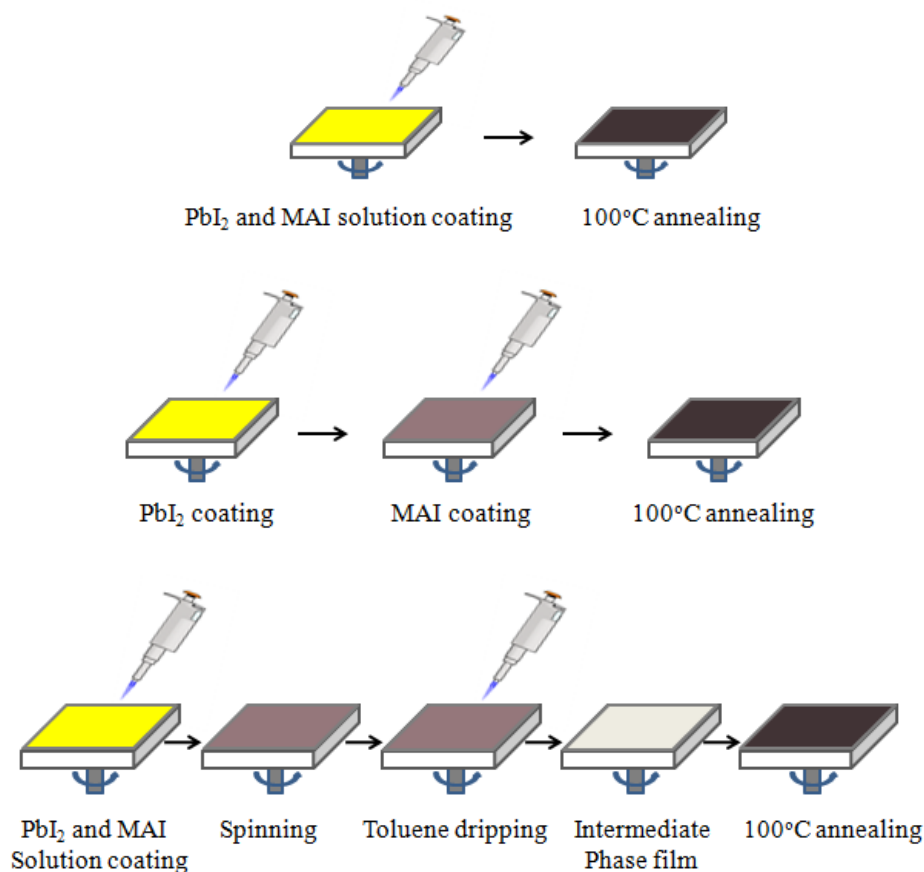


Figure 5. Perovskite processing methods including one step coating (top), two step coating (middle), and solvent engineering (bottom).

1.4 Hole transporting material (HTM) effects on OMHP PV

Spiro-OMeTAD is small molecule largely used as HTL in perovskite solar cells. Many devices with high efficiency were achieved with Spiro-OMeTAD as HTL.⁵²⁻⁵⁵ However this material has tedious synthesis process, low stability, and low charge-carrier mobility. Therefore, spiro-OMeTAD usually doped with additives like 4-tert-butylpyridine (TBP) and Li-bis-(trifluoromethanesulfonyl) imide (Li-TFSI) to increase the electrical conductivity. Using additional additives make higher cost of device processing and it degrade device performance later.⁵⁶ Recently, other materials have been reported from inorganic materials

like nickel oxide (NiO), copper iodide (CuI), copper thiocyanate (CuSCN).^{57,58} People have developed alternative HTMs with higher performance and lower cost for OMHP photovoltaic cells.⁵⁹⁻⁶³

1.5 Research objectives

Energy level alignments are vital for efficient charge extraction and collection processes in PV devices. The HTL-perovskite interface has a significant influence on charge extraction in the device. If there are interfacial defects, charges can become trapped at these low energy defects and recombine. Generally, good film morphology and crystallinity of perovskite thin films, and well aligned energy levels between layers are key factors to understand and improve to make more efficient photovoltaic cells.^{64,65} Thus, it is necessary to analyze the energy levels in order to optimize the interfaces.⁶⁶ Here, we applied eight different HTLs of varying ionization energies (IEs) and probed the device performances as a function of film morphology and HTL IE. We used nice set of different energy level materials to see the effect of IE change on OMHP PV cells. We tried modification of the HTL surface with different alcohols. We expected alcohol treatment on HTL will improve the interfacial contact between HTL and perovskite layer.

CHAPTER 2 : EXPERIMENTAL METHODS

2.1 Materials

Hydroiodic acid (HI) and lead acetate trihydrate ($\text{Pb}(\text{Ac})_2 \cdot 3\text{H}_2\text{O}$, 99.0-103.0%) were purchased from Alfa Aesar. Methylammonium bromide (MABr) was bought from Lumtec. Hole transport materials include Spiro-OMeTAD (Jilin OLED), Rubrene (TCI, >99.9%), sexithiophene (6T, TCI), N,N' -Di(1-naphthyl)- N,N' -diphenyl-(1,1'-biphenyl)-4,4'-diamine (NPD, Sigma-Aldrich, 99%), The electron transporting layers and electrodes include, [6,6]-phenyl C61-butyric acid methyl ester (PC_{61}BM , Nano-C), C60 (Nano-C, 99.5%), 2,9-dimethyl-4,7-diphenyl-1,10-phenanthroline (BCP, TCI, >99.0%) and Al (99.99%, Angstrom Engineering).

2.2 Perovskite precursor preparation

Methylammonium iodide was made by mixing methylamine (27.8 mL, 40 wt%, Alfa aesar) and hydroiodic acid (30 mL, 57 wt%, Alfa aesar) in an ice bath for 2 h. After stirring at 0 °C for 2 h, the solution was evaporated at 60 °C with a rotary evaporator, leaving only methylammonium iodide (MAI). The precipitate was washed with diethyl ether several times until the color of precipitate changed to white. The obtained precipitate was dried under vacuum for 24 h and stored in a nitrogen-filled glove box (<0.1 ppm H_2O and O_2) before use.

2.3 Inverted OMHP PV cell device preparation

ITO substrates were sequentially sonicated in soapy water (Sodium dodecyl sulfate, Sigma-Aldrich, 150 mg/ 250 mL Deionized water), deionized water, acetone, and 2-propanol each for 10 min. After N_2 blowing, substrates were exposed to ultraviolet-ozone treatment for 10 min to remove organic contaminants. PEDOT:PSS (Clevios P VP AI 4083) was spin-

coated at 5000 rpm for 30 s and then annealed on a hotplate 130 °C for 15 min. Rubrene, NPD and 6T (25 nm each) were deposited by thermal evaporation with a 1 Å/s rate at a pressure of 1×10^{-7} torr. Spiro-OMeTAD (30 mg/mL chlorobenzene), DTADIS derivatives (20 mg/mL chlorobenzene) were spin-coated at 4000 rpm for 30s and annealed at 70 °C for 5 min. The perovskite precursor was spin coated on top of the HTL. With the exception of PEDOT:PSS, all other HTLs were prepared inside a N₂-purged glove box (<0.1 ppm O₂ and H₂O). All further processing was also done in this glovebox. For alcohol treatment, 80 µm of 1-butanol was dripped on substrate and spin-coated at 4000 rpm for 30 s before perovskite layer processing. To make perovskite precursor solution, MAI and Pb(Ac)₂·3H₂O were dissolved in anhydrous DMF at 3:1 molar ratio. Final concentration of solution was 46 wt% before adding 1 mol% MABr to Pb(Ac)₂·3H₂O in DMF.⁶⁷ This solution was spin-coated at 4000 rpm for 30 s on top of different HTLs and then let dry for 15 s. During 15 s waiting, the perovskite film started to change from transparent to light brown color. Then, the substrates were put on a hotplate heated to 70 °C for 10 min. Substrate color changed rapidly to mirror like dark brown color upon putting on the hotplate. After cool down, PC₆₁BM (20 mg/mL chlorobenzene) solution was spin-coated on top of perovskite thin film at 4000 rpm for 30 s. C60 (20 nm) and BCP (10 nm) were deposited through thermal evaporation with a rate of 1 Å/s at a pressure of less than 10^{-7} torr. Finally, aluminum (100 nm) electrodes were evaporated through a shadow mask that defined 4 cells of 0.1 cm² area and 4 cells of 0.2 cm² area per substrate.

2.4 Conventional OMHP PV cell device preparation

ITO cleaning and preparation are same as mentioned previously, C60 was thermally deposited 10 nm on ITO substrate in thermal evaporator. Full device structure is

ITO/ETL/MAPbI₃/Spiro-OMeTAD/Ag. 0.1 wt% polyethylenimine (PEI, Sigma-Aldrich) was spin-coated at 5000 rpm for 30 s. Perovskite precursor solution was spin-coated as reported previously.⁵² Spiro-OMeTAD (30 mg/mL, chlorobenzene) was spin-coated at 4000 rpm for 30 s and annealed at 70 °C for 5 min inside N₂-filled glove box. After cool down substrate, it moved to thermal evaporator. 100 nm of Ag was deposited with 1 Å/s less than 10⁻⁷ torr through a shadow mask.

For TiO₂ cells, 50 µL of titanium(IV) isopropoxide (>97.0%, Sigma-Aldrich) was added to 950 µL of ethanol. 14 µL of 1M hydrochloric acid was added to solution slowly and stirred for 20 min. This mild acidic solution is deposited on ITO substrate at 5000 rpm 30s by spin-coating followed by an annealing treatment at 500 °C for 30 min.⁶⁸ 3-aminoethylphosphonic acid (10 mg/mL ethanol) solution, 0.1 wt% polyvinylpyrrolidone (PVP, Sigma-Adrich) was spin-coated at 5000 rpm 30 s. PEI, perovskite layer, spiro-OMeTAD, and Ag were prepared same way as mentioned before for C60 cell.

2.4 Instrumental background

X-ray photoelectron spectroscopy (XPS) is a surface analysis technique that measures the binding energy associated with each core atomic orbital. XPS uses x-rays with photon energies of 200 – 2000 eV to examine core levels of elements based on their characteristic binding energies. From XPS data, we can get the information about concentration of elements from intensity of peaks and information on the binding states of the elements present. This technique requires ultra high vacuum (UHV) conditions. Ultraviolet photoelectron spectroscopy (UPS) is another surface analysis technique that examines valence energy levels by using ultraviolet radiation with photon energies of 10 – 45 eV. In our system a H Lyman- α lamp with 10.2 eV photon energy is used as the excitation source. The external quantum

efficiency (EQE) for a photovoltaic device is given by the ratio of the number of electrons extracted from the device per incident photon as a function of wavelength. The EQE depends on both light absorption by the active layer and the efficiency by which these charges are collected by the electrodes.

CHAPTER 3 : OMHP PV CELL DEVICE OPTIMIZATION

3.1 Adduct solution procedure

In perovskite solar cells, inverted or conventional device architecture, a number of methods to fabricate solar cells have been reported. N. G. Park group introduced non polar diethyl ether during perovskite film processing in ambient air.⁵² They explained diethyl ether was the most reproducible solvent to form homogeneous perovskite thin film and it helped to solve the problem of rapid DMF evaporation during spin coating. To optimize film morphology conditions, during the film spinning different diethyl ether drip time were tried here. Full device architecture is ITO/PEDOT:PSS/MAPbI₃/PCBM/C60/BCP/Al. Electron transporting layers (PCBM, C60, BCP) and electrode (Al) were all fabricated according to the details of the experimental section.

Figure. 6 shows the best photovoltaic performance, which was obtained with dripping diethyl ether 5 s after the substrate started spinning. The best device gave J_{sc} of 22.38 mA/cm², V_{oc} of 0.90 V, FF of 0.65 resulting in 13.25% PCE without hysteresis. Analyzing the variation in diethyl ether drip time in J_{sc} , it is clear that current is increased with fast drip during perovskite precursor spinning. At the same time, V_{oc} and FF didn't show much variation with differing drip time. Diethyl ether drip after 5s perovskite solution spinning showed 5% increased current than after 10s. This results agree with previous reports that an earlier solvent drip plays a role to avoid fast evaporation of perovskite precursor solvent.⁵² Finally, we tried this same procedure, where the perovskite is coated in ambient atmosphere, with other HTMs. Overall, it was difficult to obtain reproducible results and some of the HTMs did not yield working devices when fabricated outside of the glovebox. These results may be explained by the variation of humidity in the atmosphere and the instability of some of the HTMs to oxygen and water.⁶⁹⁻⁷¹

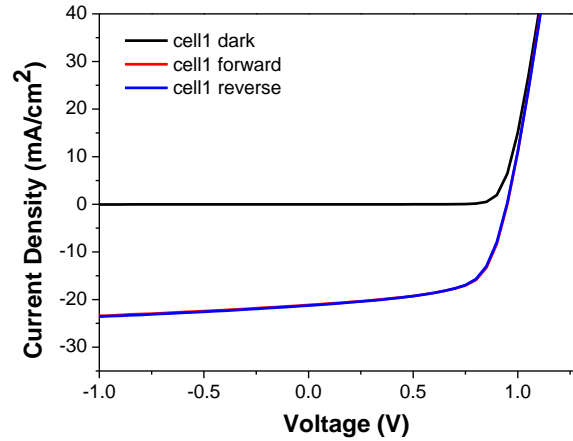


Figure 6. J-V curves of adduct solution procedure.

Table 1. PV parameters of adduct solution procedure OMHP PV cells

Cell	Ether drip	J_{sc} (mA/cm^2)	V_{oc} (V)	FF	PCE best(%)	PCE (%)
1	5s after start	22.38 ± 0.5	0.90 ± 0.01	0.65 ± 0.01	13.25	12.96 ± 0.28
2		21.12 ± 0.4	0.95 ± 0.01	0.64 ± 0.01	12.78	12.03 ± 0.15
3	10s after start	20.64 ± 0.4	0.89 ± 0.01	0.62 ± 0.01	11.35	11.07 ± 0.34
4	15s after start	18.29 ± 0.8	0.88 ± 0.01	0.61 ± 0.01	11.12	10.07 ± 1.11

3.2 Conventional architecture

Another structure of perovskite solar cells that we explored is the conventional device structure. In this structure, the perovskite thin film is deposited on top of the ETL, and then the HTL is deposited on top of the perovskite thin film. It has been reported self assembly monolayer (SAM) can incorporate with interface then change energy alignment.^{72,73} From this way of controlling the surface properties, we can expect PV cell performance

enhancement. Especially, amino group modified film surface have shown increased crystallization of perovskite film.^{43,74} Here, we study the effect of SAM which has amino group with and without on top of C60 and TiO₂ ETL.

Table 2 shows J-V characteristics of conventional cells, and the corresponding performance parameters. First, when applied different kinds of SAMs, they all showed lower FF than both C60 and TiO₂ ETL only device. C60 ETL device showed low FF with 0.48 and device PCE decreased by 48 % from best to average. For TiO₂ cells, best device gave J_{sc} of 18.70 mA/cm², V_{oc} of 1.03 V, FF of 0.74 resulting in 14.26 % PCE. Although PCE is high, average PCE is 9.35%. This is 34% difference between best and average cell PCE. These conventional architecture devices all showed large hysteresis therefore, this is not real efficiency of solar cell. PEI, PVP, and 3-aminoethylphosphonic acid layer gave working solar cells, but in conventional cells there were significant variation in the performance of the PV cells. We determined perovskite process with conventional structure with this perovskite system is not reproducible.

Table 2. PV parameters of conventional PVcells with different ETL

Cell	ETL	J _{sc} (mA/cm ²)	V _{oc} (V)	FF	PCE best(%)	PCE (%)
1	C60 (10nm)	17.97±0.8	1.05±0.05	0.48±0.02	9.11	5.22±3.7
2	C60 (10nm)/PEI	18.67±1.3	1.03±0.05	0.40±0.01	7.76	5.26±1.8
3	TiO ₂	18.70±1.1	1.03±0.06	0.74±0.02	14.26	9.35±3.8
4	TiO ₂ /PEI	11.05±0.9	1.00±0.04	0.40±0.01	4.37	1.77±2.1
5	TiO ₂ /PVP	21.25±1.5	0.97±0.05	0.45±0.02	9.24	5.53±3.6
6	TiO ₂ /3-amino ethylphosphonic acid	19.03±1.6	1.06±0.04	0.62±0.02	12.38	8.83±3.3

3.3 Comparison of methylammonium iodide (MAI)

Based on conventional cell results, we concluded that outside of glove box perovskite processing is less reproducible, and all devices discussed from here on were fabricated in the N₂-purged glove box (<0.1 ppm O₂ and H₂O).⁶⁷ Full device structure is ITO/HTL/MAPbI₃/PCBM/C60/BCP/Al. Electron transporting layers (PCBM, C60, BCP) and electrode (Al) were all fabricated according to the details of the experimental section. To further optimize the perovskite solar cells we investigated the effects of annealing temperature and MAI purchased from Lumtec vs. MAI synthesized in our lab.

Figure 7 shows the J-V curves of the perovskite cell using the types of MAI with the same perovskite processing conditions. The house MAI cell achieved a PCE of 7.2%, an J_{sc} of 13.25 mA/cm², an V_{oc} of 0.90 V, and a FF of 0.60 with 80 °C annealing for 5 min after perovskite layer spin coating. The same processing cell with Lumtec MAI achieved a PCE of 5.78%, a J_{sc} of 12.77 mA/cm², and a V_{oc} of 0.74 V, and a FF of 0.61. We found that house MAI also showed better performance with other perovskite processing conditions as well. All the photovoltaic parameters of these cells are summarized in Table 3.

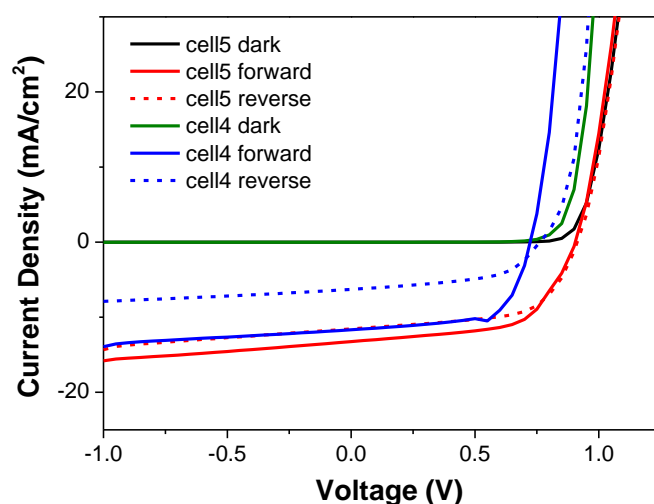


Figure 7. J-V curves of Lumtec MAI and house MAI.

Table 3. PV parameters of OMHP PV cells with different MAI, annealing temperature process

Cell	MAI	MAPbI ₃	J _{sc} (mA/cm ²)	V _{oc} (V)	FF	PCE best(%)	PCE (%)
1	Lumtec	65 °C 1min, 100 °C 2min	4.84±0.2	0.71±0.05	0.48±0.02	1.64	1.51±0.1
2	House		8.83±0.4	0.84±0.04	0.69±0.01	5.1	3.83±1.1
3	Lumtec	70 °C 5 min	11.68±0.5	0.72±0.03	0.68±0.01	5.78	4.15±0.8
4	Lumtec	80 °C 5 min	12.77±0.4	0.74±0.03	0.61±0.01	5.78	3.94±0.8
5	House		13.25±0.3	0.90±0.02	0.6±0.02	7.2	5.81±0.6
6	Lumtec	90 °C 5 min	10.33±0.4	0.71±0.04	0.63±0.02	4.63	4.14±0.4

After determining that house MAI gave better performance, we optimized the processing conditions with this MAI. As shown in Figure 8 and Table 4, 70 °C annealing temperature results in a J_{sc}, V_{oc}, and FF of 16.99 mA/cm², 0.94 V, and 62%, respectively, leading to a PCE of 9.87%. The 80 °C annealing temperature device gave a PCE of 7.68%, with a J_{sc} of 15.81 mA/cm², a V_{oc} of 0.88 V, and a FF of 55%. Accordingly, higher annealing temperatures showed lower J_{sc} and V_{oc} and resulted in lower PCE of device.

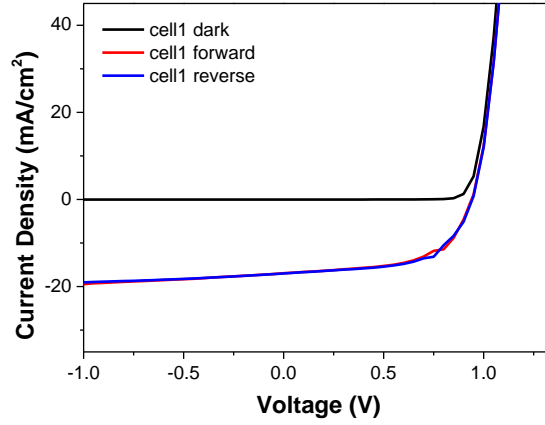


Figure 8. J-V curves of optimized OMHP PV cell.

Table 4. PV parameters of OMHP PV cells with different annealing temperature, drip solution process

Cell	MAI	MAPbI ₃	Jsc (mA/cm ²)	Voc (V)	FF	PCE (%)	PCE average (%)
1	House	70°C 5min	16.99±0.3	0.94±0.01	0.62±0.01	9.87	8.97±0.3
2		80°C 5min	15.81±0.3	0.88±0.03	0.55±0.01	7.68	6.80±0.3
3		90°C 5min	14.42±0.2	0.87±0.02	0.71±0.01	8.89	8.29±0.2
4		80°C 5min Toluene drop	15.4±0.3	0.8±0.03	0.58±0.01	7.22	6.75±0.2
5		80°C 5min diethyl ether drop	15.68±0.3	0.92±0.02	0.62±0.01	8.98	8.18±0.4

CHAPTER 4 : HTM EFFECTS ON OMHP PV PERFORMANCE

4.1 Selection of HTMs

The HTMs were selected to span a range of ionization energies that overlapped well with the valence band energy of MAPbI₃. Rubrene, NPD and 6T (see Figure 9 for chemical structures) are used as organic hole transport material in organic light emitting diodes (OLEDs) due to their good hole transporting ability.^{75,76}

Small organic molecules, such as triarylaminines are well known for its good hole transporting property and high stability.^{77,78} Especially, triphenylamine (TPA) derivatives have attracted people's attention because structure can be modified easily and has solution processable molecules as well as high hole transporting mobility.⁷⁹ DTADIS derivatives have TPA moieties on silicon core. By adding methoxy group on phenyl ring, we tried to increase solubility of molecule and tuned energy level by adding more TPA moiety on core.

4.2 Energy levels of HTMs

One of the ways to check the IEs is by using UPS. The UPS spectra were measured with a H Lyman- α (10.2 eV) source with the sample biased at -5.0 V. Figure 10 shows the UPS spectra of the different HTMs. The samples for the ionization potential measurements were prepared in the same way as described in the experimental section on top of ITO substrates without perovskite thin film. The work function (WF) of NPD, Rubrene and 6T were 4.39, 4.6, 4.0 eV respectively. The IEs of NPD, Rubrene and 6T were 5.33, 5.41 and 4.84 eV. The IE of 6T is the lowest, and these are similar values with previous reports.^{80,81} The WFs of DTADIS1, DTADIS2, and DTADIS3 were found to be 4.7, 4.44, and 4.21 eV respectively.

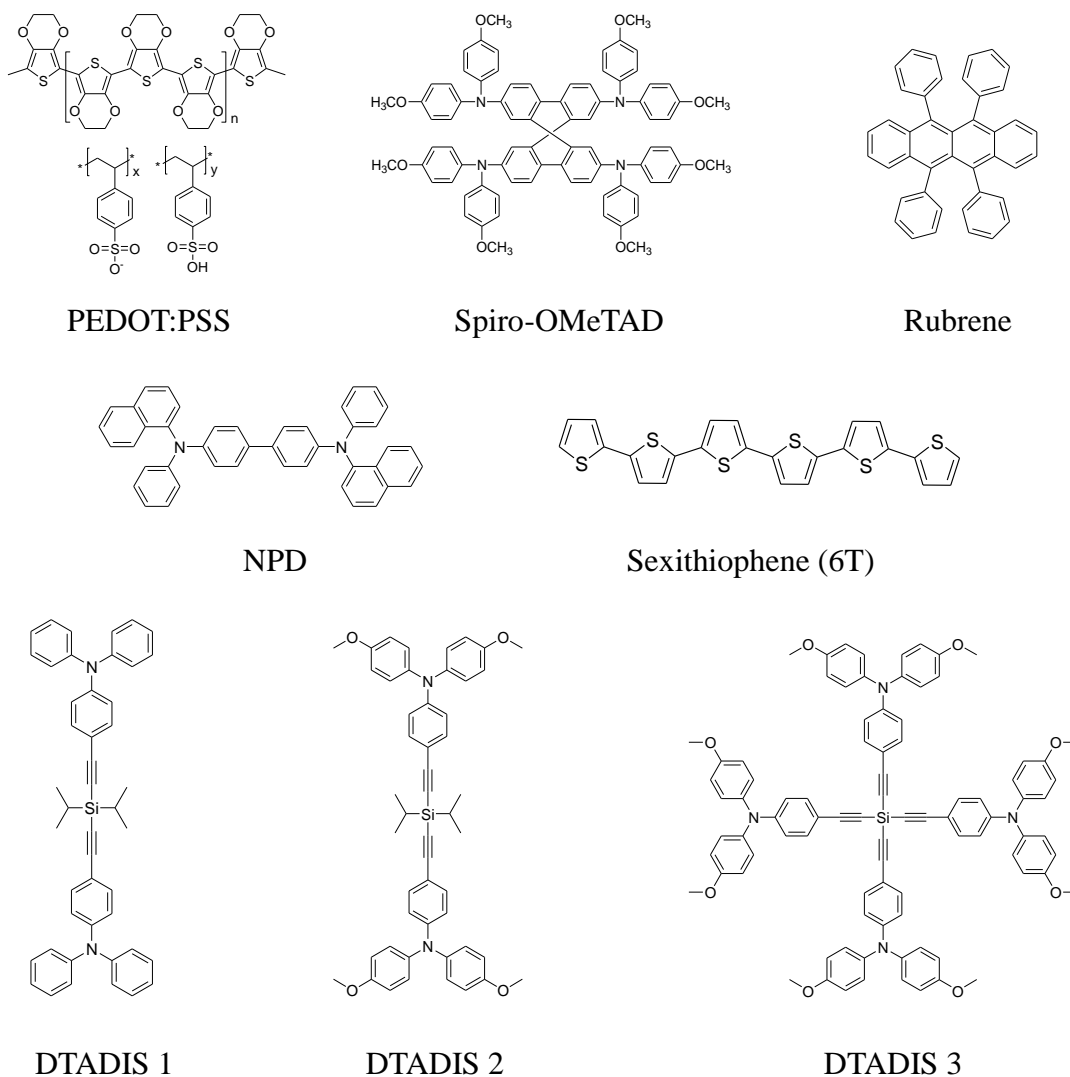


Figure 9. Chemical structure of hole transporting materials (HTMs).

DTADIS1 which has no methoxy group on the phenyl rings showed the highest ionization energy (IE) of 5.75 eV, as shown in Figure 13. The HOMO onset for DTADIS2 and 3 are similar relative to the Fermi Energy, but the IEs differ by 0.23 eV owing to the 0.22 eV difference in WFs. DTADIS1, which doesn't have methoxy groups on the phenyl rings, shows the highest IE among all the HTMs. Adding methoxy group resulted in lower IEs, as did adding more triarylamine groups. Based on UPS measurement, we could see energy level change by tuning molecular structure even in same group of derivatives.

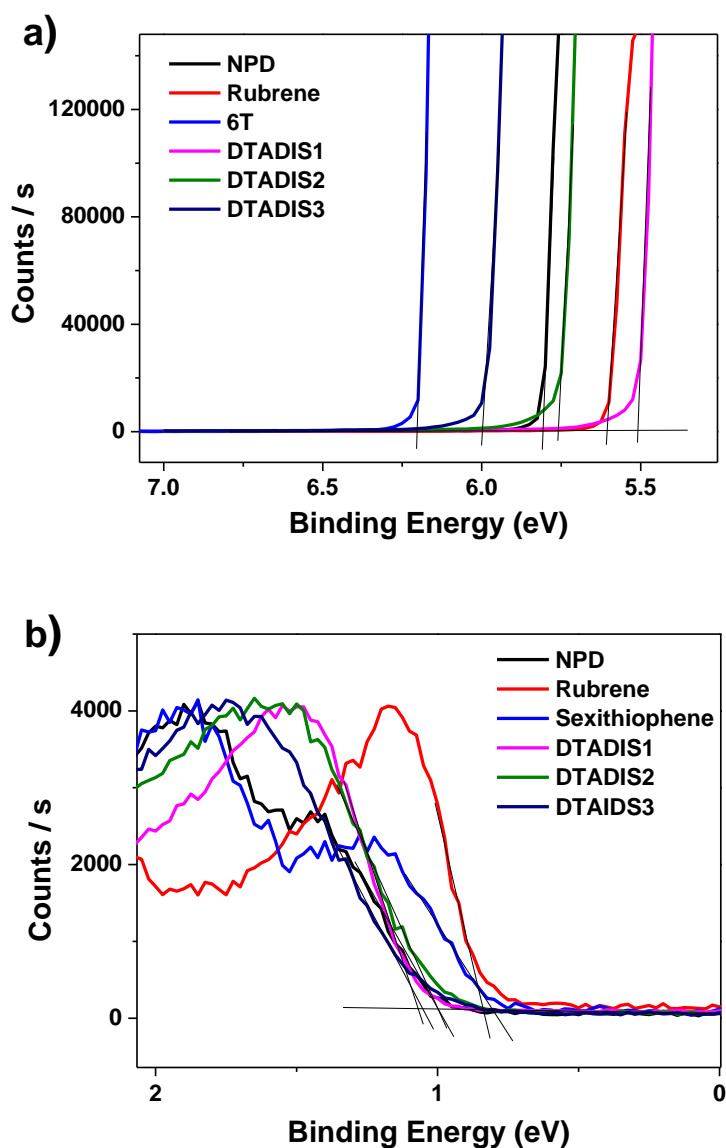


Figure 10. UPS energetic spectra for HTMs showing the a) secondary electron cutoff and b) HOMO onset region.

The schematic band alignment is sketched in Figure 11 with all different HTLs. NPD, Rubrene, 6T, DTADIS1, DTADIS2 and DTADIS3 levels are extracted from our UPS results and other values are from previous reports.⁸²⁻⁸⁴ We expect that the HTMs with transport energies close to that of the perovskite should perform best from an energetic standpoint.⁸⁵

We also predict that a slightly lower transport level in the HTM may be beneficial to drive charge transfer and reduce charge build up in the perovskite layer.⁵³ Based on these considerations, we would expect Spiro-OMeTAD, DTADIS3, NPD, Rubrene, and DTADIS2 to show the best performance. Notably, other factors, such as the charge carrier mobility and parasitic absorption by the HTM may also significantly influence HTM performance.

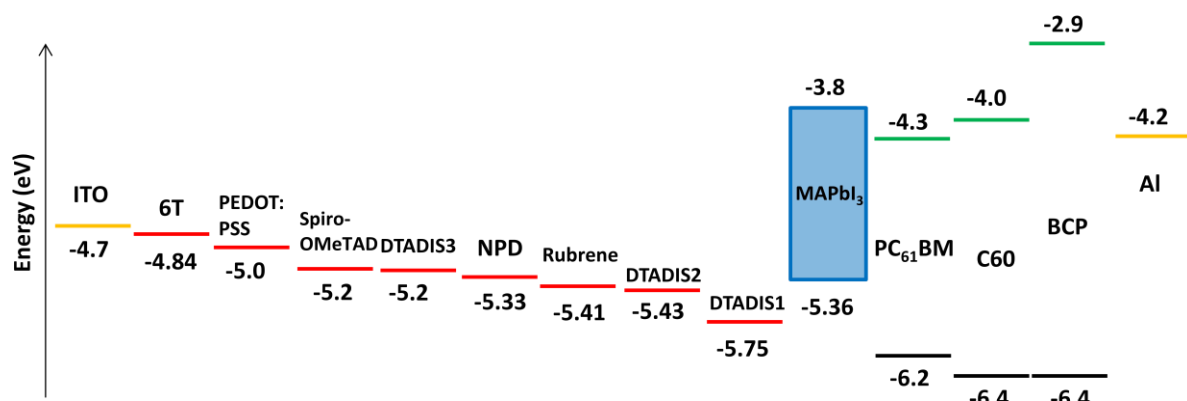


Figure 11. Schematic band alignment in OMHP PV cells.

4.3 UV-vis absorption and of HTMs

Figure 12 shows the UV-vis absorption spectra of different HTLs. Solution processed HTL films were made from 5 mg/mL solutions in chlorobenzene, and vapor deposition processed HTLs were made 25 nm thickness of the HTL deposited on top of ITO substrates. Most of the HTMs absorbed only at wavelengths shorter than 420 nm, which is beneficial as this allows the majority of the incident light to reach the perovskite. Rubrene and 6T showed strong absorbance in the visible region, with rubrene showing peaks at 495 nm and 530 nm, and 6T showing a peak at 514 nm.

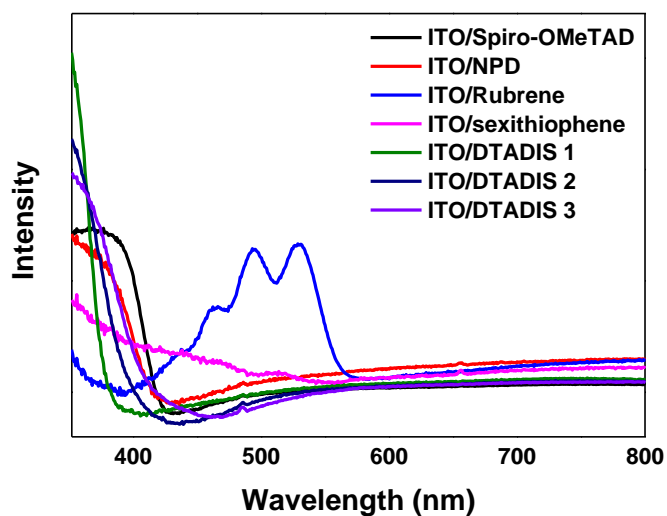


Figure 12. UV-vis absorption spectra of different HTLs.

4.4 Device performances of OMHP PV cells

As shown in Figure 13 and Table 5, photovoltaic cell parameters were measured under the irradiation of simulated AM 1.5G solar light for MAPbI₃ cells with the various HTMs. Optimized PEDOT:PSS cells showed a maximum PCE of 10.2% with a V_{oc} of 0.91 V, J_{sc} of 16.07 mA/cm², and FF of 0.69. The best Spiro-OMeTAD cell showed a 10.0% PCE with a slightly increased V_{oc} (1.01 V) and decreased J_{sc} compared to the PEDOT:PSS cell. One explanation for the increased V_{oc} observed with Spiro-OMeTAD as compared to PEDOT:PSS is the better energy level alignment. With PEDOT:PSS, it may be thought that the 5.0 eV WF is limiting the V_{oc} , whereas with Spiro-OMeTAD that 5.2 eV IE would allow for nearly a 0.2 eV higher V_{oc} . With the hypothesis that the IE of the HTM is limiting the V_{oc} , we looked at HTMs with both higher and lower IEs. Surprisingly, as displayed in Table 5, we found that the V_{oc} with 6T as an HTM, which has an IE of 4.84 eV, also showed a V_{oc} of 1.0 V. We expected NPD and rubrene will have good PV performance because of similar IE with VB of perovskite film, but those gave lower V_{oc} and J_{sc} than PEDOT:PSS.

The DTADIS derivatives provide a nice set of HTMs for comparison, as they have similar structures with varying IEs. DTADIS3 has the same IE (5.2 eV) as Spiro-OMeTAD. This can be explained slightly larger V_{oc} (0.98 V) than PEDOT:PSS which was supported by balancing IE help to increase V_{oc} of solar cell. Interestingly, for DTADIS2, it turned out higher V_{oc} and J_{sc} than rubrene although IE difference was only 0.02 eV. This means it is hard to conclude that higher V_{oc} and J_{sc} are only from well-aligned energy level. When IE increases even higher like 5.75 eV of DTADIS1, it starts to decrease photovoltaic parameters. For DTADIS1, decrease of FF to 0.49 is from S-shaped kink in JV curve. This kink can be found both forward and reverse bias scan. Consider the fact that J_{sc} of DTADIS1 is not the lowest value compare with all HTLs, lowest FF is the main reason that it gave lowest PCE. Generally, S-kink of device is from injection barrier between interfaces.^{86,87} We think 0.04 V higher IE may effected charge transfer as a injection barrier. This barrier cause charge recombination and thus decrease device efficiencies. From here, we think that HTLs with lower IEs than the perovskite film VB do not have a negative effect on PV performance, but HTLs with IEs higher than the perovskite film VB introduces a barrier to charge extraction that negatively influences PV performance.

Additionally, post solution treatment processes can improve film morphology and wetting ability. Guo et al. introduced different alcohol treatment methods on active layer.⁸⁸ They explained after solvent treatment, film morphology and optical properties were enhanced without changing thickness of active layer. We tried surface treatment with 1-butanol. Interestingly, only rubrene and DTADIS3 showed notable differences than other HTLs. All V_{oc} , J_{sc} , and FF parameters were increased resulting in higher PCE. We think alcohol played a role to wet perovskite film better, this can be studied further by looking IE change from UPS and morphology change from microscopy.

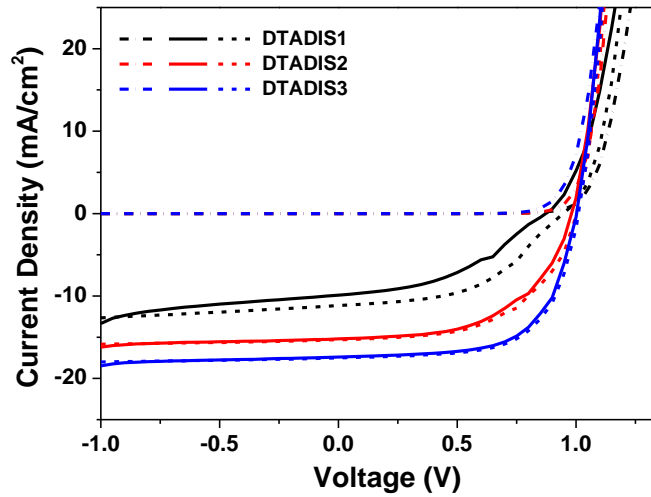
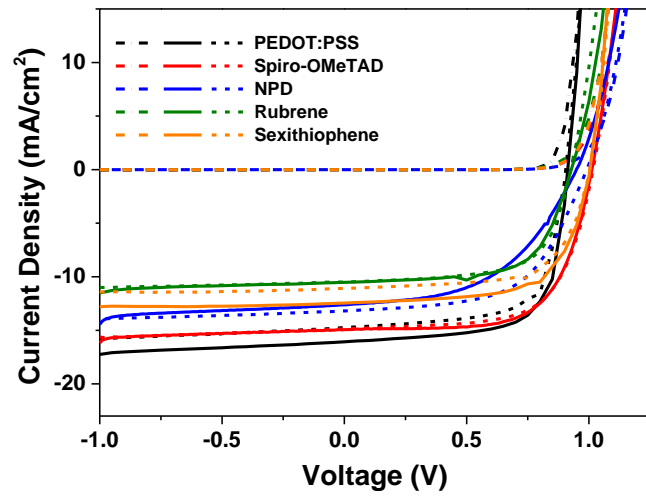


Figure 13. J-V characteristic of OMHP PV cells with different HTMs showing the dark (dash and dot), forward (solid), reverse (dash) curves.

Table 5. PV parameters of OMHP PV cells with different HTMs

Cell	HTL	MAPbI ₃	J _{sc} (mA/cm ²)	V _{oc} (V)	FF	PCE best (%)	PCE (%)
1	PEDOT:PSS	70°C 5 min	15.35±0.72	0.91±0.01	0.69±0.02	10.2	9.63±0.28
2	Spiro- OMeTAD (30mg/1mL)	70°C 5 min	14.66±0.25	1.01±0.01	0.64±0.02	10.0	9.50±0.51
3	NPD (25 nm)	70°C 5 min	11.57±0.93	0.95±0.04	0.56±0.02	7.38	6.19±0.89
4	Rubrene (25 nm)	70°C 5 min	9.01±0.90	0.88±0.02	0.57±0.03	5.22	4.48±0.49
5		1-butanol 70°C 5 min	10.50±0.64	0.93±0.02	0.66±0.02	6.37	5.4±0.71
6	Sexithiophene (25 nm)	70°C 5 min	11.38±0.56	1.01±0.01	0.65±0.02	8.40	7.48±0.48
7	DTADIS 1 (30mg/1mL)	70°C 5 min	10.29±0.83	0.92±0.04	0.46±0.03	5.14	4.43±0.74
8	DTADIS 2 (30mg/1mL)	70°C 5 min	14.71±0.19	0.98±0.01	0.54±0.02	8.23	7.83±0.34
9	DTADIS 3 (30mg/1mL)	70°C 5 min	15.48±0.22	0.98±0.01	0.62±0.02	10.05	9.45±0.48
10		1-butanol 70°C 5 min	17.42±0.67	1.00±0.01	0.64±0.02	11.41	9.37±0.85

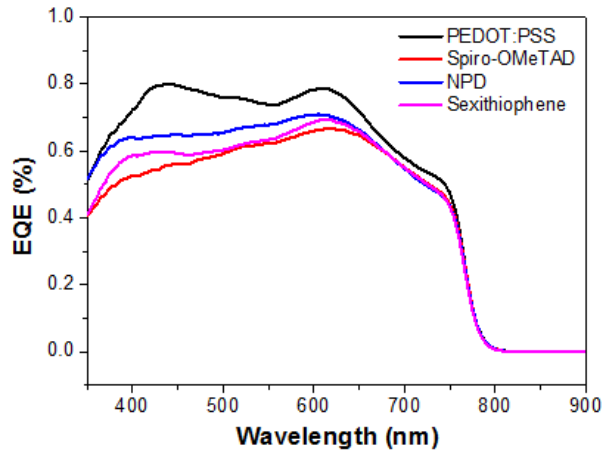


Figure 14. External quantum efficiency (EQE) spectra of OMHP PV cells.

4.5 Morphological characterization

It is well known that perovskite homogeneous morphology is essential requirement for high performance cell.^{38,39} Scanning electron microscope (SEM) was used to characterize perovskite thin film morphologies on each HTLs to see perovskite film were well coated on top of HTLs. Each samples were prepared ITO/HTL/MAPbI₃ in the same way as mentioned in device experimental section.

Top view SEM images were taken after perovskite thin film coating on top of different HTLs as shown in Figure 15. Average grain sizes of MAPbI₃ were 0.1 μm and it was well distributed without any pinholes on top of HTLs. The grain sizes of PEDOT:PSS HTL substrate were larger than other seven HTLs. From SEM images, we determined our perovskite film formed homogeneous and continuous morphology with all HTLs with results in working PV cells.

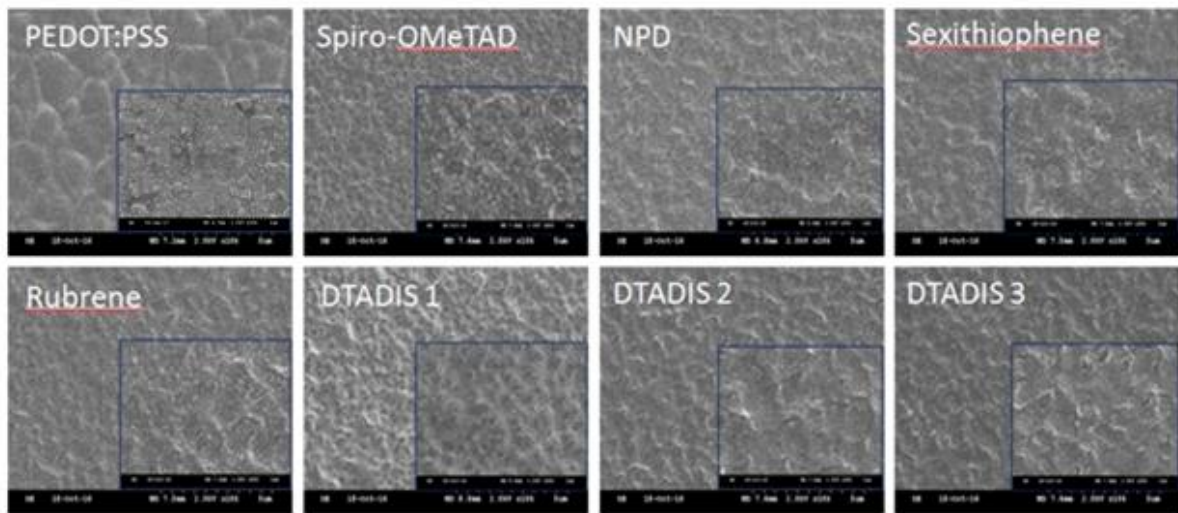


Figure 15. Scanning electron microscope (SEM) images of OMHP PV cells with 5 μm scale bar and inset images 1 μm scale bar.

CONCLUSIONS

In summary, this study tried different hole transporting materials varying energy levels to make better performance perovskite solar cells. This tells the researchers that homogeneous morphology is important to get good device and align energy level helps to improve device performances. By optimizing processing, best device with DTADIS3 gave J_{sc} of 17.5 mA/cm^2 , V_{oc} of 1.01 V, FF of 0.65 resulting in 11.41% PCE. We found that smaller IE of our HTL comparing to VB of perovskite film has small effect on efficiency of cell. However, HTLs with higher IE shows much lower PCE. Our systematic result will help to design new HTM for making better cell by aligning energy levels. We believe that not only energy level alignment but also surface treatment for wetting perovskite film will increase efficiency of photovoltaic cells.

REFERENCES

- (1) agency, I. i. e. **2015**.
- (2) Chapin, D. M.; Fuller, C. S.; Pearson, G. L. *Journal of Applied Physics* **1954**, *25*, 676.
- (3) Laboratory, N. R. E. 2015.
- (4) Sordo, S. D.; Abbene, L.; Caroli, E.; Mancini, A. M.; Zappettini, A.; Ubertini, P. *Sensors* **2009**, *9*, 3491.
- (5) Mali, M. G.; Yoon, H.; Joshi, B. N.; Park, H.; Al-Deyab, S. S.; Lim, D. C.; Ahn, S.; Nervi, C.; Yoon, S. S. *ACS Applied Materials & Interfaces* **2015**, *7*, 21619.
- (6) Henson, Z. B.; Mullen, K.; Bazan, G. C. *Nature chemistry* **2012**, *4*, 699.
- (7) Son, H. J.; Carsten, B.; Jung, I. H.; Yu, L. *Energy & Environmental Science* **2012**, *5*, 8158.
- (8) You, J.; Dou, L.; Yoshimura, K.; Kato, T.; Ohya, K.; Moriarty, T.; Emery, K.; Chen, C.-C.; Gao, J.; Li, G.; Yang, Y. *Nature Communications* **2013**, *4*, 1446.
- (9) McCulloch, I.; Ashraf, R. S.; Biniek, L.; Bronstein, H.; Combe, C.; Donaghey, J. E.; James, D. I.; Nielsen, C. B.; Schroeder, B. C.; Zhang, W. *Accounts of Chemical Research* **2012**, *45*, 714.
- (10) Zhang, X.; Xu, Y.; Giordano, F.; Schreier, M.; Pellet, N.; Hu, Y.; Yi, C.; Robertson, N.; Hua, J.; Zakeeruddin, S. M.; Tian, H.; Grätzel, M. *Journal of the American Chemical Society* **2016**, *138*, 10742.
- (11) Yum, J.-H.; Hagberg, D. P.; Moon, S.-J.; Karlsson, K. M.; Marinado, T.; Sun, L.; Hagfeldt, A.; Nazeeruddin, M. K.; Grätzel, M. *Angewandte Chemie* **2009**, *121*, 1604.
- (12) Park, S. M.; Yoon, Y.; Jeon, C. W.; Kim, H.; Ko, M. J.; Lee, D.-K.; Kim, J. Y.; Son, H. J.; Kwon, S.-K.; Kim, Y.-H.; Kim, B. *Journal of Polymer Science Part A: Polymer Chemistry* **2014**, *52*, 796.
- (13) Liu, X.; Liebermann, R. C. *Physics and Chemistry of Minerals* **1993**, *20*, 171.
- (14) Papavassiliou, G. C. *Molecular Crystals and Liquid Crystals Science and Technology. Section A. Molecular Crystals and Liquid Crystals* **1996**, *286*, 231.
- (15) Zhou, A. J.; Zhu, T. J.; Zhao, X. B. *Materials Science and Engineering: B* **2006**, *128*, 174.
- (16) Koji, Y.; Hiroshi, K.; Takashi, M.; Tsutomu, O.; Sumio, I. *Bulletin of the Chemical Society of Japan* **1990**, *63*, 2521.
- (17) Kim, H.-S.; Lee, C.-R.; Im, J.-H.; Lee, K.-B.; Moehl, T.; Marchioro, A.; Moon, S.-J.; Humphry-Baker, R.; Yum, J.-H.; Moser, J. E.; Grätzel, M.; Park, N.-G. *Scientific Reports* **2012**, *2*, 591.
- (18) Collavini, S.; Völker, S. F.; Delgado, J. L. *Angewandte Chemie International Edition* **2015**, *54*, 9757.
- (19) Beal, R. E.; Slotcavage, D. J.; Leijtens, T.; Bowring, A. R.; Belisle, R. A.; Nguyen, W. H.; Burkhard, G. F.; Hoke, E. T.; McGehee, M. D. *The Journal of Physical Chemistry Letters* **2016**, *7*, 746.
- (20) Zhumekenov, A. A.; Saidaminov, M. I.; Haque, M. A.; Alarousu, E.; Sarmah, S. P;

Murali, B.; Dursun, I.; Miao, X.-H.; Abdelhady, A. L.; Wu, T.; Mohammed, O. F.; Bakr, O. M. *ACS Energy Letters* **2016**, *1*, 32.

(21) Kojima, A.; Teshima, K.; Shirai, Y.; Miyasaka, T. *Journal of the American Chemical Society* **2009**, *131*, 6050.

(22) Liu, M.; Johnston, M. B.; Snaith, H. J. *Nature* **2013**, *501*, 395.

(23) Noh, J. H.; Im, S. H.; Heo, J. H.; Mandal, T. N.; Seok, S. I. *Nano Letters* **2013**, *13*, 1764.

(24) Werner, J.; Weng, C.-H.; Walter, A.; Fesquet, L.; Seif, J. P.; De Wolf, S.; Niesen, B.; Ballif, C. *The Journal of Physical Chemistry Letters* **2016**, *7*, 161.

(25) Park, B.-w.; Jain, S. M.; Zhang, X.; Hagfeldt, A.; Boschloo, G.; Edvinsson, T. *ACS Nano* **2015**, *9*, 2088.

(26) Im, J.-H.; Jang, I.-H.; Pellet, N.; Grätzel, M.; Park, N.-G. *Nat Nano* **2014**, *9*, 927.

(27) Liu, D.; Gangishetty, M. K.; Kelly, T. L. *Journal of Materials Chemistry A* **2014**, *2*, 19873.

(28) Motta, C.; El-Mellouhi, F.; Sanvito, S. *Scientific Reports* **2015**, *5*, 12746.

(29) Ke, W.; Zhao, D.; Grice, C. R.; Cimaroli, A. J.; Fang, G.; Yan, Y. *Journal of Materials Chemistry A* **2015**, *3*, 23888.

(30) Kim, J.; Kim, G.; Kim, T. K.; Kwon, S.; Back, H.; Lee, J.; Lee, S. H.; Kang, H.; Lee, K. *Journal of Materials Chemistry A* **2014**, *2*, 17291.

(31) Ke, W.; Fang, G.; Liu, Q.; Xiong, L.; Qin, P.; Tao, H.; Wang, J.; Lei, H.; Li, B.; Wan, J.; Yang, G.; Yan, Y. *Journal of the American Chemical Society* **2015**, *137*, 6730.

(32) Liu, D.; Kelly, T. L. *Nat Photon* **2014**, *8*, 133.

(33) Wu, C.-G.; Chiang, C.-H.; Tseng, Z.-L.; Nazeeruddin, M. K.; Hagfeldt, A.; Gratzel, M. *Energy & Environmental Science* **2015**, *8*, 2725.

(34) Park, I. J.; Park, M. A.; Kim, D. H.; Park, G. D.; Kim, B. J.; Son, H. J.; Ko, M. J.; Lee, D.-K.; Park, T.; Shin, H.; Park, N.-G.; Jung, H. S.; Kim, J. Y. *The Journal of Physical Chemistry C* **2015**, *119*, 27285.

(35) Huang, C.; Liu, C.; Di, Y.; Li, W.; Liu, F.; Jiang, L.; Li, J.; Hao, X.; Huang, H. *ACS Applied Materials & Interfaces* **2016**, *8*, 8520.

(36) Liu, C.; Wang, K.; Du, P.; Meng, T.; Yu, X.; Cheng, S. Z. D.; Gong, X. *ACS Applied Materials & Interfaces* **2015**, *7*, 1153.

(37) Marinova, N.; Tress, W.; Humphry-Baker, R.; Dar, M. I.; Bojinov, V.; Zakeeruddin, S. M.; Nazeeruddin, M. K.; Grätzel, M. *ACS Nano* **2015**, *9*, 4200.

(38) Wu, Y.; Chen, W.; Yue, Y.; Liu, J.; Bi, E.; Yang, X.; Islam, A.; Han, L. *ACS Applied Materials & Interfaces* **2015**, *7*, 20707.

(39) Mao, P.; Zhou, Q.; Jin, Z.; Li, H.; Wang, J. *ACS Applied Materials & Interfaces* **2016**, *8*, 23837.

(40) Chen, Q.; Zhou, H.; Hong, Z.; Luo, S.; Duan, H.-S.; Wang, H.-H.; Liu, Y.; Li, G.; Yang,

Y. *Journal of the American Chemical Society* **2014**, *136*, 622.

(41) Kim, G.-W.; Kim, J.; Lee, G.-Y.; Kang, G.; Lee, J.; Park, T. *Advanced Energy Materials* **2015**, *5*, n/a.

(42) Xu, B.; Bi, D.; Hua, Y.; Liu, P.; Cheng, M.; Gratzel, M.; Kloo, L.; Hagfeldt, A.; Sun, L. *Energy & Environmental Science* **2016**, *9*, 873.

(43) Zuo, L.; Gu, Z.; Ye, T.; Fu, W.; Wu, G.; Li, H.; Chen, H. *Journal of the American Chemical Society* **2015**, *137*, 2674.

(44) Chang, C.-Y.; Chu, C.-Y.; Huang, Y.-C.; Huang, C.-W.; Chang, S.-Y.; Chen, C.-A.; Chao, C.-Y.; Su, W.-F. *ACS Applied Materials & Interfaces* **2015**, *7*, 4955.

(45) Wang, D.; Liu, Z.; Zhou, Z.; Zhu, H.; Zhou, Y.; Huang, C.; Wang, Z.; Xu, H.; Jin, Y.; Fan, B.; Pang, S.; Cui, G. *Chemistry of Materials* **2014**, *26*, 7145.

(46) Xiao, Z.; Bi, C.; Shao, Y.; Dong, Q.; Wang, Q.; Yuan, Y.; Wang, C.; Gao, Y.; Huang, J. *Energy & Environmental Science* **2014**, *7*, 2619.

(47) Su, T.-S.; Hsieh, T.-Y.; Hong, C.-Y.; Wei, T.-C. *Scientific Reports* **2015**, *5*, 16098.

(48) Cui, D.; Yang, Z.; Yang, D.; Ren, X.; Liu, Y.; Wei, Q.; Fan, H.; Zeng, J.; Liu, S. *The Journal of Physical Chemistry C* **2016**, *120*, 42.

(49) Burschka, J.; Pellet, N.; Moon, S.-J.; Humphry-Baker, R.; Gao, P.; Nazeeruddin, M. K.; Gratzel, M. *Nature* **2013**, *499*, 316.

(50) Jeon, N. J.; Noh, J. H.; Kim, Y. C.; Yang, W. S.; Ryu, S.; Seok, S. I. *Nat Mater* **2014**, *13*, 897.

(51) Li, W.; Fan, J.; Li, J.; Mai, Y.; Wang, L. *Journal of the American Chemical Society* **2015**, *137*, 10399.

(52) Ahn, N.; Son, D.-Y.; Jang, I.-H.; Kang, S. M.; Choi, M.; Park, N.-G. *Journal of the American Chemical Society* **2015**, *137*, 8696.

(53) Zhou, H.; Chen, Q.; Li, G.; Luo, S.; Song, T.-b.; Duan, H.-S.; Hong, Z.; You, J.; Liu, Y.; Yang, Y. *Science* **2014**, *345*, 542.

(54) Xu, B.; Tian, H.; Bi, D.; Gabrielsson, E.; Johansson, E. M. J.; Boschloo, G.; Hagfeldt, A.; Sun, L. *Journal of Materials Chemistry A* **2013**, *1*, 14467.

(55) Li, H.; Fu, K.; Hagfeldt, A.; Grätzel, M.; Mhaisalkar, S. G.; Grimsdale, A. C. *Angewandte Chemie International Edition* **2014**, *53*, 4085.

(56) Berhe, T. A.; Su, W.-N.; Chen, C.-H.; Pan, C.-J.; Cheng, J.-H.; Chen, H.-M.; Tsai, M.-C.; Chen, L.-Y.; Dubale, A. A.; Hwang, B.-J. *Energy & Environmental Science* **2016**, *9*, 323.

(57) Christians, J. A.; Fung, R. C. M.; Kamat, P. V. *Journal of the American Chemical Society* **2014**, *136*, 758.

(58) Chavhan, S.; Miguel, O.; Grande, H.-J.; Gonzalez-Pedro, V.; Sanchez, R. S.; Barea, E. M.; Mora-Sero, I.; Tena-Zaera, R. *Journal of Materials Chemistry A* **2014**, *2*, 12754.

(59) Wang, H.; Sheikh, A. D.; Feng, Q.; Li, F.; Chen, Y.; Yu, W.; Alarousu, E.; Ma, C.; Haque, M. A.; Shi, D.; Wang, Z.-S.; Mohammed, O. F.; Bakr, O. M.; Wu, T. *ACS Photonics* **2015**, *2*,

849.

(60) Wu, Q.; Xue, C.; Li, Y.; Zhou, P.; Liu, W.; Zhu, J.; Dai, S.; Zhu, C.; Yang, S. *ACS Applied Materials & Interfaces* **2015**, *7*, 28466.

(61) Chen, H.; Bryant, D.; Troughton, J.; Kirkus, M.; Neophytou, M.; Miao, X.; Durrant, J. R.; McCulloch, I. *Chemistry of Materials* **2016**, *28*, 2515.

(62) Huang, C.; Fu, W.; Li, C.-Z.; Zhang, Z.; Qiu, W.; Shi, M.; Heremans, P.; Jen, A. K. Y.; Chen, H. *Journal of the American Chemical Society* **2016**, *138*, 2528.

(63) Kang, M. S.; Sung, S. D.; Choi, I. T.; Kim, H.; Hong, M.; Kim, J.; Lee, W. I.; Kim, H. K. *ACS Applied Materials & Interfaces* **2015**, *7*, 22213.

(64) Salim, T.; Sun, S.; Abe, Y.; Krishna, A.; Grimsdale, A. C.; Lam, Y. M. *Journal of Materials Chemistry A* **2015**, *3*, 8943.

(65) Tsai, H.; Nie, W.; Cheruku, P.; Mack, N. H.; Xu, P.; Gupta, G.; Mohite, A. D.; Wang, H.-L. *Chemistry of Materials* **2015**, *27*, 5570.

(66) Zhou, Z.; Pang, S.; Liu, Z.; Xu, H.; Cui, G. *Journal of Materials Chemistry A* **2015**, *3*, 19205.

(67) Zhao, L.; Luo, D.; Wu, J.; Hu, Q.; Zhang, W.; Chen, K.; Liu, T.; Liu, Y.; Zhang, Y.; Liu, F.; Russell, T. P.; Snaith, H. J.; Zhu, R.; Gong, Q. *Advanced Functional Materials* **2016**, *26*, 3508.

(68) Eperon, G. E.; Burlakov, V. M.; Docampo, P.; Goriely, A.; Snaith, H. J. *Advanced Functional Materials* **2014**, *24*, 151.

(69) Guo, Q.; Li, C.; Qiao, W.; Ma, S.; Wang, F.; Zhang, B.; Hu, L.; Dai, S.; Tan, Z. a. *Energy & Environmental Science* **2016**, *9*, 1486.

(70) Lee, D.-Y.; Na, S.-I.; Kim, S.-S. *Nanoscale* **2016**, *8*, 1513.

(71) Jiang, Y.; Li, C.; Liu, H.; Qin, R.; Ma, H. *Journal of Materials Chemistry A* **2016**, *4*, 9958.

(72) Gu, Z.; Zuo, L.; Larsen-Olsen, T. T.; Ye, T.; Wu, G.; Krebs, F. C.; Chen, H. *Journal of Materials Chemistry A* **2015**, *3*, 24254.

(73) Beaumont, N.; Hancox, I.; Sullivan, P.; Hatton, R. A.; Jones, T. S. *Energy & Environmental Science* **2011**, *4*, 1708.

(74) Xia, F.; Wu, Q.; Zhou, P.; Li, Y.; Chen, X.; Liu, Q.; Zhu, J.; Dai, S.; Lu, Y.; Yang, S. *ACS Applied Materials & Interfaces* **2015**, *7*, 13659.

(75) Jia, W.; Chen, Q.; Chen, L.; Yuan, D.; Xiang, J.; Chen, Y.; Xiong, Z. *The Journal of Physical Chemistry C* **2016**, *120*, 8380.

(76) Jou, J.-H.; Shen, S.-M.; Tsai, Y.-C. *ACS Applied Materials & Interfaces* **2011**, *3*, 3134.

(77) Liu, S.; Jiang, X.; Ma, H.; Liu, M. S.; Jen, A. K. Y. *Macromolecules* **2000**, *33*, 3514.

(78) Mohamed, S.; Demeter, D.; Laffitte, J.-A.; Blanchard, P.; Roncali, J. *Scientific Reports* **2015**, *5*, 9031.

(79) Leliège, A.; Blanchard, P.; Rousseau, T.; Roncali, J. *Organic Letters* **2011**, *13*, 3098.

- (80) Chang, J.-H.; Lin, W.-H.; Wang, P.-C.; Taur, J.-I.; Ku, T.-A.; Chen, W.-T.; Yan, S.-J.; Wu, C.-I. *Scientific Reports* **2015**, *5*, 9693.
- (81) Gassmann, J.; Yampolskii, S. V.; Genenko, Y. A.; Reusch, T. C. G.; Klein, A. *The Journal of Physical Chemistry C* **2016**, *120*, 10466.
- (82) Wang, K.; Liu, C.; Du, P.; Zheng, J.; Gong, X. *Energy & Environmental Science* **2015**, *8*, 1245.
- (83) Wang, C.; Turinske, A. J.; Gao, Y. *Applied Physics B* **2013**, *113*, 361.
- (84) Wang, Z.; Yokoyama, D.; Wang, X.-F.; Hong, Z.; Yang, Y.; Kido, J. *Energy & Environmental Science* **2013**, *6*, 249.
- (85) Belisle, R. A.; Jain, P.; Prasanna, R.; Leijtens, T.; McGehee, M. D. *ACS Energy Letters* **2016**, *1*, 556.
- (86) Tress, W.; Leo, K.; Riede, M. *Advanced Functional Materials* **2011**, *21*, 2140.
- (87) Wagenpfahl, A.; Rauh, D.; Binder, M.; Deibel, C.; Dyakonov, V. *Physical Review B* **2010**, *82*, 115306.
- (88) Guo, S.; Cao, B.; Wang, W.; Moulin, J.-F.; Müller-Buschbaum, P. *ACS Applied Materials & Interfaces* **2015**, *7*, 4641.

VITA

EDUCATION

2007-2011

B. S. Department of Material Science and Engineering, Gyeongsang National University, Jinju, South Korea, Advisor: Professor. Soon-Ki Kwon

2011-2013

M. S. Department of Material Science and Engineering, Gyeongsang National University, Jinju, South Korea, Advisor: President. Soon-Ki Kwon, Professor. Joung-Man Park

Thesis Title: "Synthesis and Characterization of Organic Semiconducting Polymers and Oligomers for OTFT and OPV"

CAREERS

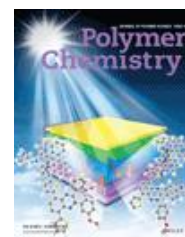
2011-2013 SAMSUNG DISPLAY OLED center researcher

2013-2014 Engineering Research Institute researcher, Gyeongsang National University

PUBLICATIONS

[10] H. G. Song, Y. B. Kim, **S. M. Park**, T. K. An, S. K. Kwon, C. E. Park, Y. H. Kim, 'Synthesis, characterization, and transistor applications of new linear molecules: Naphthayl-ethynyl-anthracene-based small molecules containing different alkyl end group' *Dyes and Pigments*, **2016**, 131, 349-355

[9] **S. M. Park**, Y. Yoon, C. W. Jeon, H. Kim, M. J. Kim, D. K. Lee, J. Y. Kim, H. J. Son, S. K. Kwon, Y. H. Kim, B. S. Kim, 'Synthesis of Phenanthro[1,10,9,8-cdefg]carbazole-based Conjugated Polymers for Organic Solar Cell Applications' *Journal of Polymer Science: Part A*, **2014**, 52, 6, 796-803. (front cover article)



[8] **S. M. Park**, H. N. Kim, S. C. Shin, Y. H. Kim, 'New Semiconducting Copolymers Containing Alkyl Quaterthiophene and Alkoxy Naphthalene Moieties for Organic Thin Film Transistors' *Macromolecular Research*, **2014**, 22, 9, 1012-1017.

[7] **S. M. Park**, I. Kang, Y. L. Yu, S. Y. Nam, J. Hwang, Y. H. Kim, 'Organic Semiconductor Based on Asymmetric Naphthalene-Thiophene Molecule for Organic Thin Film Transistors' *Journal of Nanoscience and Nanotechnology*, **2014**, 14, 8, 6172-6176.

- [6] H. J. Yun, M. C. Hwang, **S. M. Park**, R. Kim, D. S. Chung, Y. H. Kim, S. K. Kwon, 'Synthesis of a Low-Bandgap Fluorinated Donor-Acceptor Copolymer and Its Optoelectronic Application' *ACS Applied Materials & Interfaces*, **2013**, 5, 6045-6053.
- [5] T. K. An,** **S. M. Park**,** S. Nam, J. Hwang, S. J. Yoo, M. J. Lee, W. M. Yun, J. Jang, H. Cha, J. Hwang, S. Park, J. Kim, D. S. Chung, Y. H. Kim, S. K. Kwon, C. E. Park, 'Thin Film Morphology Control via a Mixed Solvent System for High-Performance Organic Thin Film Transistors' *Science of Advanced Materials*, **2013**, 5, 1323-1327. (** equal contribution)
- [4] I. Kang, **S. M. Park**, D. H. Lee, S. H. Han, D. S. Chung, Y. H. Kim, S. K. Kwon, 'Novel Unsymmetric Oligomers Based on Benzo[d,d']Thieno[3,2-b:4,5-b']Dithiophenes for Solution-Processed Organic Field-Effect Transistors' *Science of Advanced Materials*, **2013**, 5, 1-10.
- [3] **S. M. Park**, I. Kang, H. J. Yun, S. Y. Nam, J. Hwang, Y. H. Kim, 'New Si-Based Material with Pyridopyrazine Substituents' *Bull. Korean. Chem. Soc.* **2012**, 33, 3469-3472.
- [2] S. O. Kim, K. Thangaraju, S. Jung, W. Lu, **S. M. Park**, J. Lee, J. I. Lee, H. Y. Chu, Y. H. Kim, S. K. Kwon, 'Highly Efficient Phosphorescent Organic Light Emitting Diodes Based on Iridium(III) Complex with Bulky Substituent Spacers' *Journal of Nanoscience and Nanotechnology*, **2012**, 12, 4375-4378.
- [1] S. O. Kim, M. W. Lee, S. H. Jang, **S. M. Park**, J. W. Park, M. H. Park, S. H. Kang, Y. H. Kim, C. K. Song, S. K. Kwon, 'Organic semiconductor based on phenylethynyl end-capped anthracene' *Thin Solid Films*, **2011**, 519, 7998-8002.